Hindawi
Journal of Chemistry
Volume 2019, Article ID 7851416, 9 pages
https://doi.org/10.1155/2019/7851416

Research Article

Large Specific Surface Area Macroporous Nanocast $LaFe_{1-x}Ni_xO_3$: A Stable Catalyst for Catalytic Methane Dry Reforming

Chunfeng Chen,[1] Zhaojun Meng,[1] and Zijun Wang [1,2]

[1]*School of Chemistry and Chemical Engineering, Shihezi University, Shihezi 832003, China*
[2]*Key Laboratory for Green Processing of Chemical Engineering of Xinjiang Bingtuan Shihezi University, Shihezi 832003, China*

Correspondence should be addressed to Zijun Wang; wzj_tea@shzu.edu.cn

Received 3 March 2019; Revised 20 September 2019; Accepted 18 October 2019; Published 21 December 2019

Academic Editor: Zhong-Wen Liu

Macroporous nanocast perovskites, $LaFe_{1-x}Ni_xO_3$ ($x = 0.3$, 0.5, and 0.7), were synthesized by using a nanocasting technique with SBA-15 as a template and applied to methane dry reforming (MDR). The prepared catalysts were characterized by X-ray diffraction, transmission electron microscopy, specific-surface-area analysis, hydrogen temperature-programmed reduction, and thermogravimetric analysis. $LaFe_{1-x}Ni_xO_3$ revealed a large specific surface area, which could enhance its catalytic activity. The catalysts were reduced to Ni/$LaFeO_3$-La_2O_3 in the MDR reaction. The alkaline additive, La_2O_3, and perovskite oxide, $LaFeO_3$, strongly interacted with the active component to reduce the surface energy of metal particles and prevent aggregation of active Ni. The results showed that $LaFe_{0.5}Ni_{0.5}O_3$ and $LaFe_{0.3}Ni_{0.7}O_3$ perform better than $LaFe_{0.7}Ni_{0.3}O_3$. More importantly, $LaFe_{0.5}Ni_{0.5}O_3$ had a very long lifetime (>80 h) in the MDR reaction. The $LaFe_{0.5}Ni_{0.5}O_3$ catalyst showed excellent stability in the MDR reaction and has potential use in industrial applications.

1. Introduction

The extensive use of traditional energy sources has led to the production of large amounts of CO_2, leading to two main global problems: an energy crisis and environmental pollution. Scientific researchers are currently seeking methods to solve these two issues [1–4]. Ongoing breakthroughs in the technology of shale gas extraction imply that natural gas, which comprises mostly CH_4, can be expected to replace coal as the second most abundant fossil fuel. CH_4 dry reforming (MDR, $CH_4 + CO_2 \longrightarrow 2H_2 + 2CO$) has recently received increased attention [3, 5]. The reaction simultaneously converts two greenhouse gases (CO_2 and CH_4) into syngas (H_2 and CO), which reduces the amount of the former gases in the atmosphere. Syngas is mainly applied as a fuel or feedstock in the chemical industry. Therefore, the MDR reaction presents positive environmental benefits as well as efficient energy conversion and utilization [6–9].

Noble metals and Ni-based and Co-based catalysts are commonly used in the MDR reaction [4, 10–15]. Although noble metal catalysts possess excellent catalytic activity, stability, and anti-C deposition capability, they are expensive and limited because they are difficult to use on a large scale. By comparison, Ni-based catalysts are inexpensive and can achieve catalytic effects comparable with those of noble metal catalysts by employing different carriers, additives, and preparation methods; hence, they are considered to be among the most promising industrial catalysts. However, Ni-based catalysts tend to become deactivated when subjected to long-term reactions due to C deposition and the sintering of Ni grains. Therefore, resistance to C deposition and prevention of Ni particle sintering must be studied [13, 16–24].

Perovskite-type oxides (PTOs) have shown great potential as precursors for the catalytic reformation of CH_4 and CO_2 [3, 15, 25–33]. PTO has the general formula ABO_3, wherein A is usually a La-based ion or a second main-group metal ion and B is usually a transition metal ion. PTOs have good tunability and thermodynamic and chemical stabilities. Previous studies have reported the use of perovskite-type

catalysts for MDR. Gallego et al., for example, prepared $LaNiO_3$ as a catalyst precursor; the material featured small highly dispersed Ni particles supported on La_2O_3 during the MDR reaction and exhibited high catalytic activity [34]. Despite this achievement, however, two issues were uncovered: the small surface area ($<10\ m^2 \cdot g^{-1}$) of the oxide affects its potential applications and the perovskite structure of $LaNiO_3$ is completely decomposed during the MDR reaction [5, 26]. Such perovskite decomposition results in the weakening of the interactions between Ni and the carrier, leading to Ni sintering and C scattering. One method to solve the sintering problem is to scatter the PTOs over a material with a large specific surface area, thermal stability, and metal sintering resistance, such as ordered SBA-15 silica [35–37]. The issue of C deposition has been considered in recent studies, which have shown that controlling the $LaNiO_3$ precursor or partial substitution of Ni-containing perovskites largely suppresses Ni sintering and C deposition. Partial substitution of Ni by Fe in $LaNiO_3$ stabilizes the perovskite structure by providing stronger metal-support interactions and maintaining a larger specific surface area [9, 28]; thus, it allows the catalyst to endure the MDR reaction.

In this study, we synthesized large specific surface area macroporous $LaFe_{1-x}Ni_xO_3$ perovskite-type catalysts by using nanocatalyst technology and SBA-15 as a template. The prepared catalysts enabled the thorough dispersion of active Ni and showed high catalytic activity. Active Ni strongly interacts with the carrier to prevent the growth of Ni grains, thereby remarkably improving the stability of the prepared catalysts. The activity of $LaFe_{1-x}Ni_xO_3$ during MDR was examined.

2. Materials and Methods

2.1. Catalyst Preparation

2.1.1. Preparation of Ordered SBA-15 Silica. SBA-15 silica was synthesized according to a previously reported method [35, 37–39]. Briefly, 4.0 g of P123 (Aldrich, typical Mn = 5800) was dissolved in HCl (60 g, 4 M) and 90 ml of distilled water with stirring at 40°C for 4 h. Subsequently, 8.5 g of tetraethylorthosilicate was added to the solution, which was then kept at 40°C for 22 h. The solution was transferred to a Teflon bottle and crystallized at 100°C for 24 h. Finally, the product was washed to pH 7, filtered, dried, and calcined at 550°C for 7 h.

2.1.2. Synthesis of Macropore Perovskites. The synthesized SBA-15 was used as a template to synthesize macroporous $LaFe_{1-x}Ni_xO_3$ [36, 39]. First, 1.5 g of SBA-15 was dissolved in 15 ml of distilled water for 30 min to obtain a suspension solution. Then, lanthanum nitrate, iron nitrate, nickel nitrate, and citric acid were added to citric acid dissolved in 20 mL of ethanol. The molar ratio of metal ions in the solution of La : Fe : Ni was $1 : 1 - x : x$, where $x = 0.3$, 0.5, or 0.7. The prepared suspension solution was added to this mixture and stirred at 80°C until a gelatinous solid formed. This solid was dried at 110°C for 24 h and calcined at 750°C for 7 h. Finally, 2 M NaOH aqueous solution was added to the solids 3-4 times with stirring to remove the silica template. The obtained samples were washed to pH 7 with deionized water and ethanol and dried at 100°C for 10 h. The catalysts obtained via this nanocasting method were designated as $LaFe_{1-x}Ni_xO_3$ ($x = 0.3$, 0.5, and 0.7). For comparison, $LaFe_{1-x}Ni_xO_3$ was also synthesized by following the same protocol described above but without addition of the SBA-15 template. The prepared perovskite was designated as CA-$LaFe_{1-x}Ni_xO_3$ (Scheme 1).

2.2. Characterization of Catalysts. X-ray diffraction (XRD) experiments were conducted on an X-ray diffractometer. Hydrogen temperature-programmed reduction (H_2-TPR) of the catalysts was performed with an Auto Chem 2720 catalyst characterization system (Micromeritics Instrument Corporation, USA). Thermogravimetric/differential scanning calorimetry (TG/DSC) was performed on a TA SDT Q600 system (USA). Transmission electron microscopy (TEM) was conducted on a FEI Tecnai G2 F20 instrument (USA). The BET testing was performed on an ASAP 2460 instrument.

2.3. Catalytic Performance Tests. The MDR reactions were conducted in a fixed-bed reactor. The reactor was loosely filled with 75 mg of the $LaFe_{1-x}Ni_x0_3$ catalysts and fed a mixture of CH_4, CO_2, and N_2 ($CH_4 : CO_2 : N_2 = 1.3 : 1.3 : 1$, GHSV = 30000 $mL \cdot h^{-1} \cdot gcat$). The catalytic tests were performed from 550°C to 850°C. The effluent product gases were analyzed by a GC-9790 gas chromatograph with a thermal conductivity detector. The stability tests were also conducted at 800°C for 80 h.

Conversions and H_2/CO were calculated according to the following equations [40, 41]:

$$\text{conversion of } CH_4 = \frac{[CH_4]_{in} - [CH_4]_{out}}{[CH_4]_{in}},$$

$$\text{conversion of } CO_2 = \frac{[CO_2]_{in} - [CO_2]_{out}}{[CO_2]_{in}}, \quad (1)$$

$$\frac{H_2}{CO} = \frac{[H_2]_{out}}{[CO]_{out}},$$

where "in" represents the amount of a substance in the feed gas and "out" represents the amount of a substance in the gaseous effluent.

3. Results and Discussion

3.1. Physicochemical Properties of the Catalysts. The XRD patterns of the prepared $LaFeO_3$ and $LaFe_{1-x}Ni_xO_3$ catalysts are presented in Figure 1. Catalysts prepared by the nanocasting technique exhibited a single-phase crystalline perovskite structure. All peaks observed were consistent with those of the perovskite crystals of $LaFeO_3$ (PDF#75-439) [42, 43]. The well-resolved and highly intense peaks reveal the excellent crystalline structures of the $LaFe_{1-x}Ni_xO_3$ catalysts. As x increased in $LaFe_{1-x}Ni_xO_3$, the

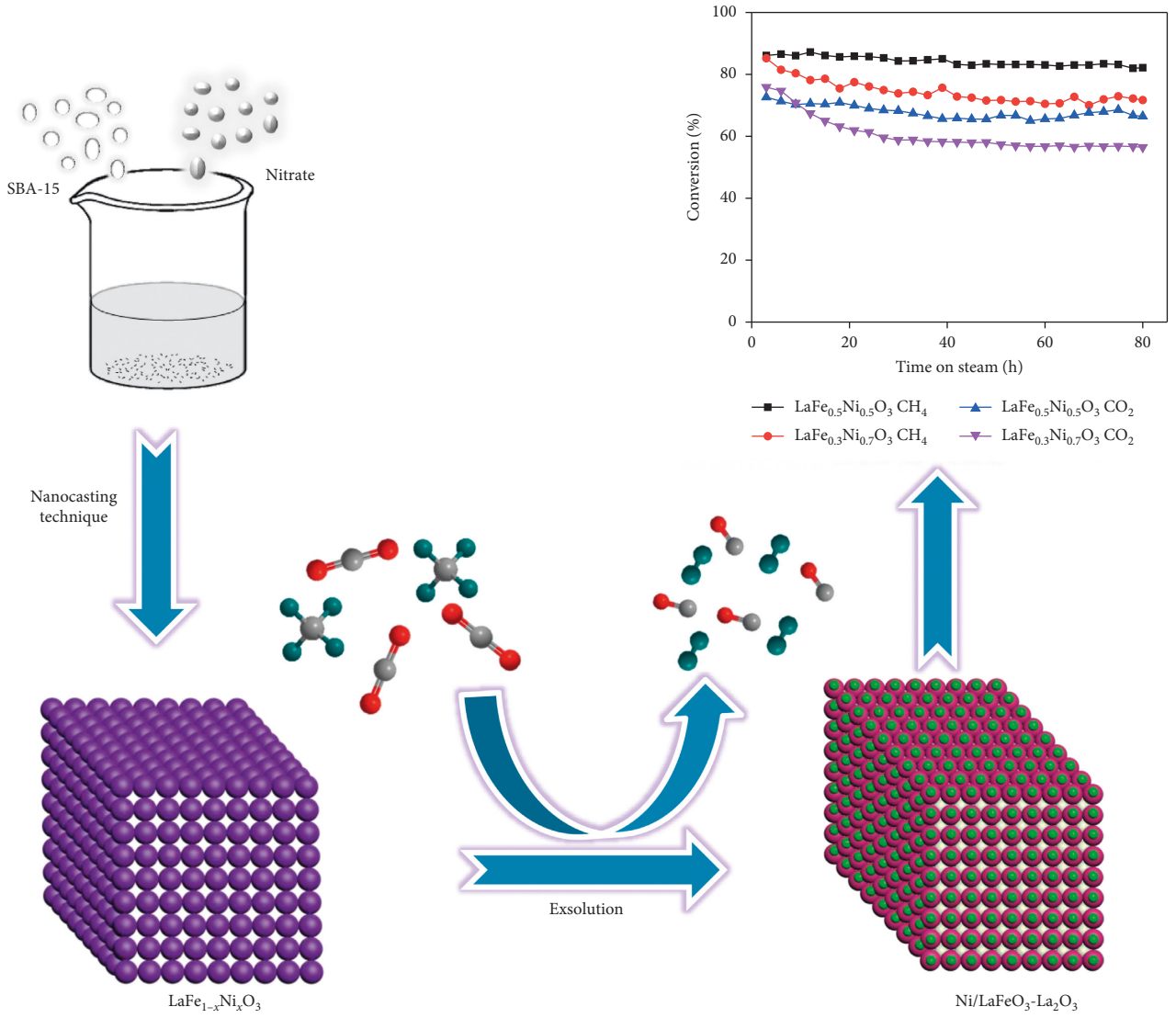

Scheme 1: Schematic diagram of the catalyst preparation.

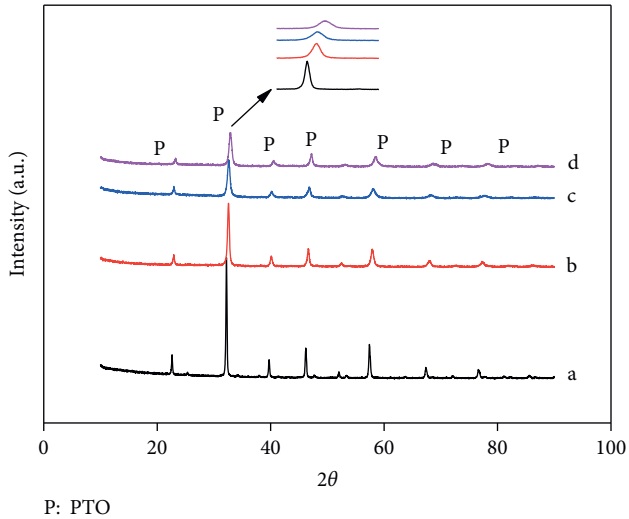

Figure 1: XRD patterns of (a) $LaFeO_3$, (b) $LaFe_{0.7}Ni_{0.3}O_3$, (c) $LaFe_{0.5}Ni_{0.5}O_3$, and (d) $LaFe_{0.3}Ni_{0.7}O_3$.

catalysts exhibited broader, lower-intensity peaks that shifted toward higher 2θ values. This result can be explained by the fact that Ni^{3+} ions in $LaFe_{1-x}$ Ni_xO_3 are in the low-spin state and smaller than the high-spin state Fe^{3+} ions. Replacing Fe^{3+} in $LaFeO_3$ with Ni^{3+} leads to a decrease in the crystal plane spacing of the PTO, which corresponds to the shift of the diffraction peaks toward higher 2θ values.

The TPR profiles of $LaFe_{1-x}$ Ni_xO_3 ($x = 0.3$, 0.5, 0.7) are shown in Figure 2. $LaFe_{0.7}Ni_{0.3}O_3$ in the 375–550°C range shows two main reduction peaks. The first peak indicates that Ni^{3+} is reduced to Ni^{2+}, while the second peak represents the reduction of Ni^{2+} to Ni^0. Interactions between Ni and Fe complicate the reduction of perovskite and lead to expansion of the second peak, thus showing a strong interaction between the active Ni and carrier [2]. $LaFe_{0.5}Ni_{0.5}O_3$ exhibits nearly the same trend as $LaFe_{0.7}Ni_{0.3}O_3$, thus suggesting that both catalysts have similar structures. Interestingly, the Ni^{3+} and Ni^{2+} reduction peaks of $LaFe_{0.3}Ni_{0.7}O_3$ move toward higher temperatures (415–750°C). This phenomenon is quite

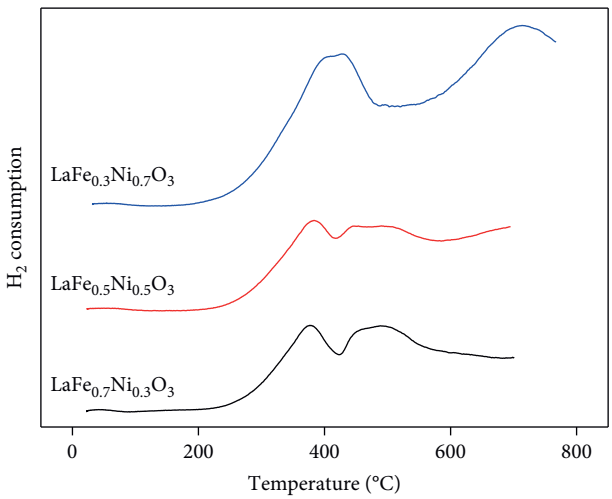

FIGURE 2: H_2-TPR profiles of $LaFe_{1-x}$ Ni_xO_3 ($x = 0.3$, 0.5, and 0.7).

different from the findings of a previous report; thus, $LaFe_{0.3}Ni_{0.7}O_3$ may have reduction intermediates different from those of $LaFe_{0.7}Ni_{0.3}O_3$ and $LaFe_{0.5}Ni_{0.5}O_3$ as the interaction between Ni and La/Fe species is likely to be altered as the Ni content increases [42–44].

As shown in Table 1, the macroporous nanocast $LaFe_{1-x}Ni_xO_3$ catalysts have significantly larger specific surface areas than the uncast CA-$LaFe_{1-x}Ni_xO_3$. Among the catalysts prepared, $LaFe_{0.5}Ni_{0.5}O_3$ showed the highest specific surface area. The improved textural characteristics of $LaFe_{1-x}Ni_xO_3$ are attributed to the templating effect of SBA-15 during perovskite synthesis [39]. Because the prepared catalyst has a large specific surface area, dispersion of the active metal of the catalyst could be greatly improved. The porous structure of the catalyst also improves its activity and stability.

3.2. Catalytic Performance. The initial catalytic activity of the $LaFe_{1-x}Ni_xO_3$ samples was tested to study the effect of Ni content on catalytic performance. In Figure 3(a) and 3(b), the conversion rates of CO_2 and CH_4 increased significantly at elevated reaction temperatures, thus displaying the endothermic feature of MDR [2, 7]. The CH_4 and CO_2 conversion rates of $LaFe_{0.5}Ni_{0.5}O_3$ and $LaFe_{0.3}Ni_{0.7}O_3$ indicated higher catalytic performance compared with that of $LaFe_{0.7}Ni_{0.3}O_3$ at 550–850°C. This finding could be attributed to the Ni content of the catalysts. Further, the CO_2 conversion was over 80%, which is higher than that of CH_4, suggesting the RWGS reaction ($CO_2 + H_2 \longrightarrow H_2O + CO$). $LaFe_{0.5}Ni_{0.5}O_3$ and $LaFe_{0.3}Ni_{0.7}O_3$ exhibit nearly the same catalytic performance at 550–850°C. The Ni content of $LaFe_{0.3}Ni_{0.7}O_3$ is higher than that of $LaFe_{0.5}Ni_{0.5}O_3$ (Figure 3), but $LaFe_{0.3}Ni_{0.7}O_3$ does not display greater activity than $LaFe_{0.5}Ni_{0.5}O_3$. This finding may be explained by the decomposition of the perovskite structure of $LaFe_{0.3}Ni_{0.7}O_3$ during the reaction; this decomposition reduces the specific surface area of the catalyst and promotes agglomeration of Ni species. The high activity of $LaFe_{0.5}Ni_{0.5}O_3$ may be due to its stable perovskite structure and high dispersion of active Ni.

3.3. XRD Patterns after Catalytic Performance. The XRD patterns of $LaFe_{1-x}Ni_xO_3$ ($x = 0.3$, 0.5, 0.7) after reduction and the MDR reaction are shown in Figure 4. No significant characteristic diffraction peak of Ni (111) was observed at 44.7° (PDF#1-1260) in the XRD patterns of the $LaFe_{1-x}Ni_xO_3$ catalysts in Figure 4(a) after reduction at 600°C for 2 h, which suggests that active Ni is highly dispersive with particles in small size. Among the three catalysts, $LaFe_{0.7}Ni_{0.3}O_3$ and $LaFe_{0.5}Ni_{0.5}O_3$ clearly maintain a good perovskite structure (Figures 4(a) and 4(b)), which reveals their high stability. After the reduction of $LaFe_{1-x}Ni_xO_3$ (Table 2), $LaFe_{0.5}Ni_{0.5}O_3$ shows the largest specific surface area, which means this catalyst has the best perovskite structure and Ni dispersion among the prepared catalysts. On the basis of the Scherrer formula (Figure 4(b)), the average particle sizes of the Ni phase of $LaFe_{0.5}Ni_{0.5}O_3$ and $LaFe_{0.3}Ni_{0.7}O_3$ were calculated to be 12.3 and 16.5 nm, respectively. The particle size of active Ni in $LaFe_{0.5}Ni_{0.5}O_3$ is relatively small; thus, the catalyst could be expected to have a long lifetime [45]. No obvious diffraction peak of Ni was found in $LaFe_{0.7}Ni_{0.3}O_3$, which performs very poorly in the activity test. Overall, Figure 4 reveals that $LaFe_{0.5}Ni_{0.5}O_3$ maintains a stable perovskite structure and smaller Ni particle size compared with the other catalysts after reduction and MDR; thus, this catalyst possesses excellent catalytic activity and stability.

3.4. Stability of the $LaFe_{0.5}Ni_{0.5}O_3$ and $LaFe_{0.3}Ni_{0.7}O_3$ Catalysts. Based on the XRD images and BET data of the three $LaFe_{1-x}Ni_xO_3$ catalysts, $LaFe_{0.5}Ni_{0.5}O_3$ and $LaFe_{0.3}Ni_{0.7}O_3$ were selected and their stabilities were tested at 800°C for 80 h (Figure 5). The results illustrate that $LaFe_{0.5}Ni_{0.5}O_3$ exhibits long-term stability than $LaFe_{0.3}Ni_{0.7}O_3$. The CH_4 and CO_2 conversion rates of $LaFe_{0.5}Ni_{0.5}O_3$ remained stable, and no significant deactivation was detected throughout the 80 h stability test; by contrast, the activity of $LaFe_{0.3}Ni_{0.7}O_3$ was significantly reduced during the stability test. Deactivation of Ni-based catalysts during MDR is mainly caused by C deposition and sintering of activated Ni grains. Ni grain size is a critical factor determining the performance of the catalyst, and smaller-sized Ni particles can effectively prevent C deposition and sintering, thereby facilitating the dry reformation of CH_4. TEM and XRD analyses reveal that the size of Ni grains on the surface of $LaFe_{0.5}Ni_{0.5}O_3$ remains small size after 80 h of testing. Figure 5 demonstrates that the H_2/CO molar ratio $LaFe_{0.5}Ni_{0.5}O_3$ of the produced syngas is close to 1, and the syngas is used as a raw material for the Fischer–Tropsch reaction. Therefore, we can conclude that the prepared mesoporous nanocast perovskite $LaFe_{0.5}Ni_{0.5}O_3$ catalyst shows good resistance to carbon deposition and has promising prospect for future applications [45, 46].

3.5. Catalyst Characterization after Stability Test. Figure 6 reveals the XRD patterns of $LaFe_{0.5}Ni_{0.5}O_3$ and $LaFe_{0.3}Ni_{0.7}O_3$ after a long period of stability testing. The XRD pattern of $LaFe_{0.5}Ni_{0.5}O_3$ (curve a) indicates a good perovskite structure, which means the prepared catalyst has good stability. By contrast, the perovskite structure of $LaFe_{0.3}Ni_{0.7}O_3$ (curve b) is completely destroyed. This

Table 1: Textural properties of the prepared catalysts.

Sample	Surface area ($m^2 \cdot g^{-1}$)	Pore volume ($cm^3\ g^{-1}$)	Pore size (nm)
CA-$LaFe_{0.7}Ni_{0.3}O_3$	3	—	—
CA-$LaFe_{0.5}Ni_{0.5}O_3$	4	—	—
CA-$LaFe_{0.3}Ni_{0.7}O_3$	2	—	—
$LaFe_{0.7}Ni_{0.3}O_3$	61	0.15	101.93
$LaFe_{0.5}Ni_{0.5}O_3$	66	0.14	86.04
$LaFe_{0.3}Ni_{0.7}O_3$	59	0.13	85.97

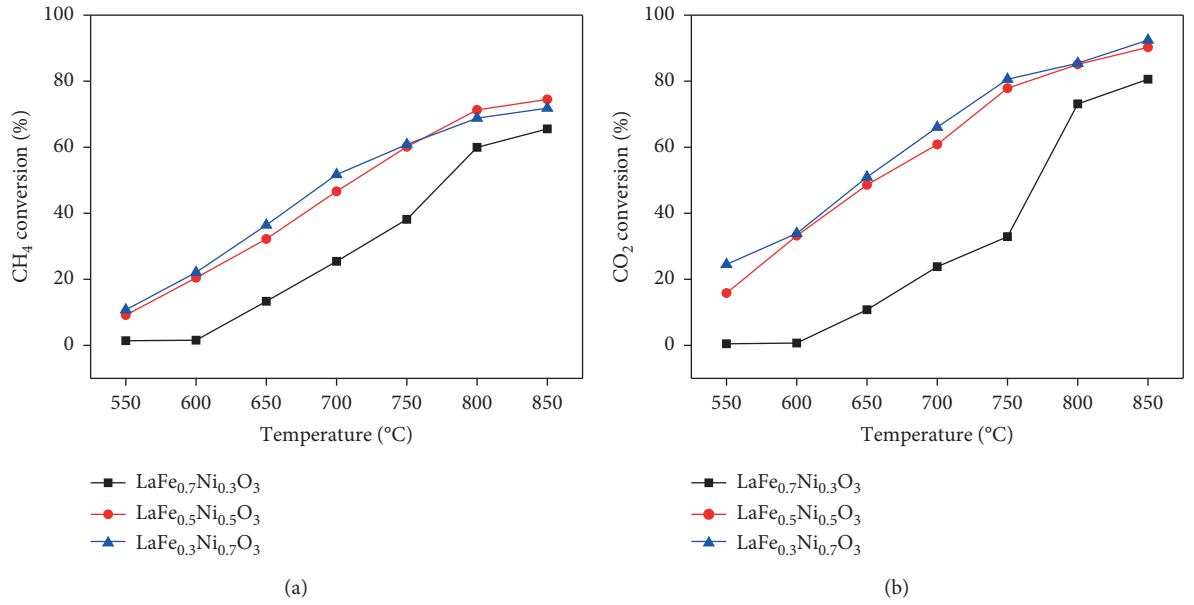

Figure 3: The conversions of CH_4 (a) and CO_2 (b) at different temperatures ($CH_4 : CO_2 : N_2 = 1.3 : 1.3 : 1$, GHSV = 30,000 mL h^{-1}·gcat).

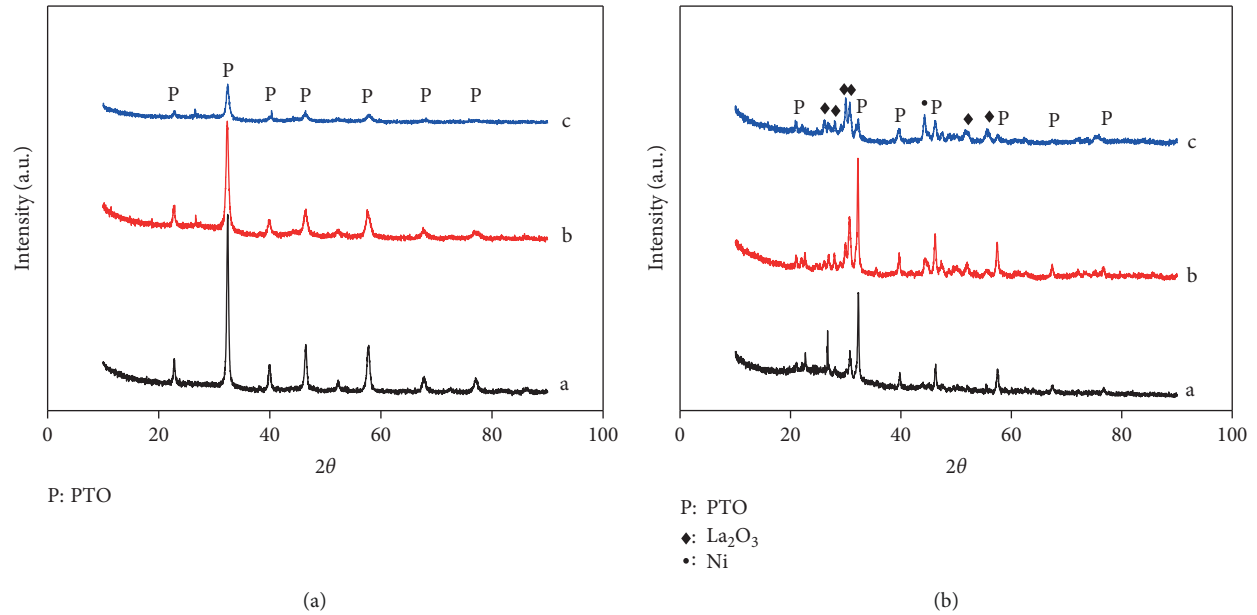

Figure 4: XRD patterns of (a) $LaFe_{1-x}Ni_xO_3$ after reduction at 600°C for 2 h in 5%H_2/95%Ar and (b) after the MDR reaction. (a) $LaFe_{0.7}Ni_{0.3}O_3$, (b) $LaFe_{0.5}Ni_{0.5}O_3$, and (c) $LaFe_{0.3}Ni_{0.7}O_3$.

Table 2: Textural properties of the catalysts after reduction at 600°C.

Sample	Surface area ($m^2 \cdot g^{-1}$)	Pore volume ($cm^3\ g^{-1}$)	Pore size (nm)
$LaFe_{0.7}Ni_{0.3}O_3$	26	0.07	112.66
$LaFe_{0.5}Ni_{0.5}O_3$	33	0.07	84.8
$LaFe_{0.3}Ni_{0.7}O_3$	15	0.06	156.90

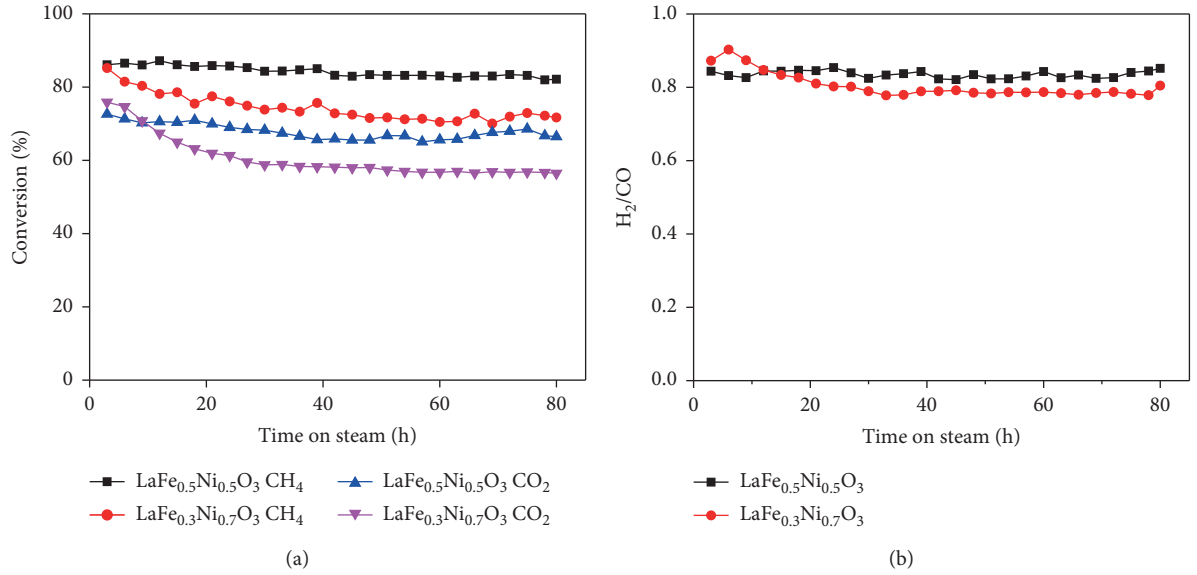

Figure 5: Variations in the conversion of $LaFe_{0.5}Ni_{0.5}O_3$ and $LaFe_{0.3}Ni_{0.7}O_3$ and H_2/CO as a function of reaction time ($T = 800°C$, $CH_4 : CO_2 : N_2 = 1.3 : 1.3 : 1$, GHSV = 30,000 mL h^{-1}·gcat).

finding may be explained by the catalyst's inability to maintain a large specific surface area, which clearly reduces its stability. In Table 3, $LaFe_{0.5}Ni_{0.5}O_3$ has a larger specific surface area and smaller Ni particle size than $LaFe_{0.3}Ni_{0.7}O_3$. These features indicate that the former can effectively limit the growth of Ni grains and thus has good sintering and carbon deposition resistance.

Figures 7(a) and 7(b) show the TEM images of $LaFe_{0.5}Ni_{0.5}O_3$ in different stages. In Figure 7(a), small and relatively uniform Ni grains may be observed on the reduced catalyst [11, 47, 48]. This result demonstrates the good dispersion of Ni grains on the surface of $LaFeO_3$. Figure 7(b) presents the catalyst after the 80 h MDR test; no significant carbon deposition could be found, which shows the good resistance of the catalyst to carbon deposition [1]. The Ni particle size is very small, consistent with the XRD results, especially after the stability test; thus, sintering of Ni grains does not occur during the MDR reaction. $LaFe_{0.5}Ni_{0.5}O_3$ revealed good resistance to carbon deposition and sintering; thus, the catalyst possesses excellent stability.

The TG/DSC profiles of $LaFe_{0.5}Ni_{0.5}O_3$ and $LaFe_{0.3}Ni_{0.7}O_3$ are shown in Figures 8(a) and 8(b). During TG testing, at first, the small weight gains may due to the adsorption of oxygen on the oxygen vacancies of the PTO surface or from the oxidation of metallic Ni particles. Two distinct exothermic peaks could be observed in the DSC profile, which means two types of C are deposited in Ni active sites. The weight loss peak at low

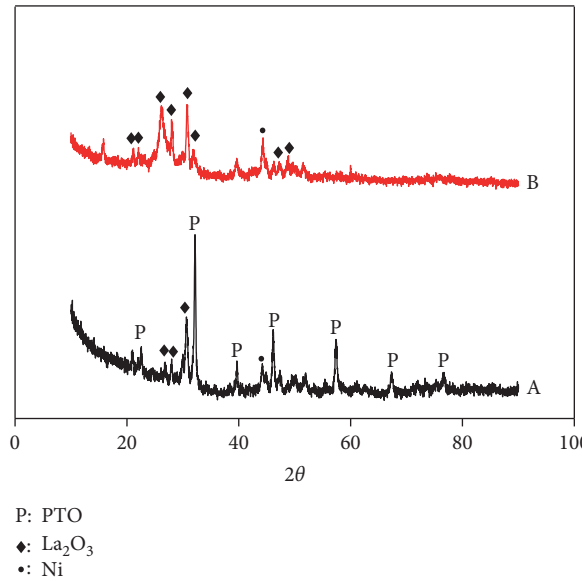

Figure 6: XRD patterns of (A) $LaFe_{0.5}Ni_{0.5}O_3$ and (B) $LaFe_{0.3}Ni_{0.7}O_3$ after stability testing.

temperatures (250–350°C) can be attributed to the oxidation of active C (α-C), which is an active species in the MDR reaction [7, 27]. The mass loss of $LaFe_{0.5}Ni_{0.5}O_3$ is 1.2%, while that of $LaFe_{0.3}Ni_{0.7}O_3$ is very small. The mass loss at high temperatures (>550°C) can be ascribed to oxidation of inert C

Table 3: Textural properties of the catalysts after stability test.

Sample	Surface area ($m^2 \cdot g^{-1}$)	Pore volume ($cm^3\ g^{-1}$)	Pore size (nm)	Particle sizes of Ni (nm)
$LaFe_{0.5}Ni_{0.5}O_3$	2	0.09	158.25	16.7
$LaFe_{0.3}Ni_{0.7}O_3$	8	—	—	24.0
Ni particle size calculated by the Scherrer method				

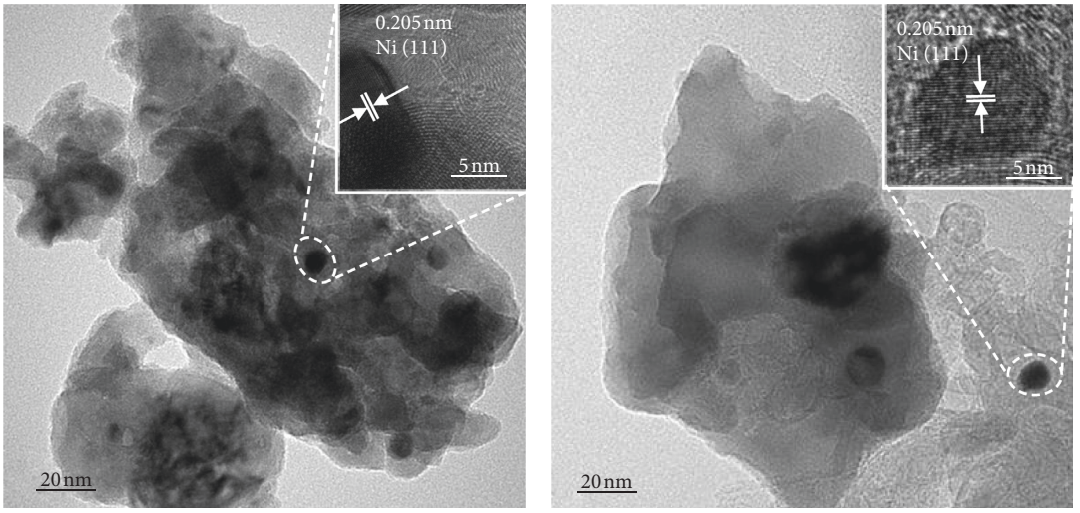

(a) (b)

Figure 7: The TEM images of $LaFe_{0.5}Ni_{0.5}O_3$ (a) after the reduction and (b) after stability test.

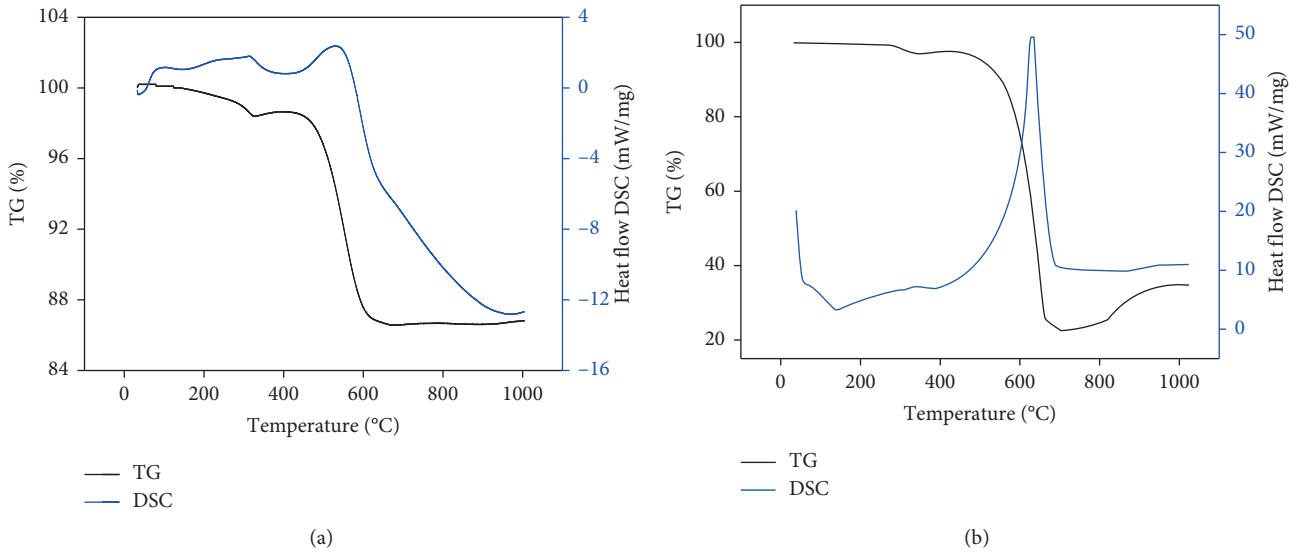

(a) (b)

Figure 8: TG-DSC profile of $LaFe_{0.5}Ni_{0.5}O_3$ (a) and $LaFe_{0.3}Ni_{0.7}O_3$ (b) after the 80 h stability test in MDR.

(γ-C), which is a major factor in catalyst deactivation. The mass loss of $LaFe_{0.5}Ni_{0.5}O_3$ is approximately 13%, while that of $LaFe_{0.3}Ni_{0.7}O_3$ is very large. $LaFe_{0.5}Ni_{0.5}O_3$ remained highly active after the 80 h stability test, and the data indicated the remarkable inhibition of C deposition on the surface of the prepared catalysts.

4. Conclusion

In summary, a series of $LaFe_{1-x}Ni_xO_3$ perovskite-type catalysts were prepared, among which $LaFe_{0.5}Ni_{0.5}O_3$ exhibited the highest activity in MDR. The prepared catalysts had a large specific surface area, which could improve their

catalytic activity. The catalysts showed excellent stability at 800°C during the MDR reaction with no significant deactivation over 80 h. The XRD, TEM, and TG-DSC data revealed no significant increase in the size of the Ni particles and no obvious carbon deposition on the catalyst after a long period of stability testing. These results demonstrate the promising application prospects of the $LaFe_{0.5}Ni_{0.5}O_3$ catalyst.

Data Availability

The data used to support the findings of this study are available from the corresponding author upon request.

Conflicts of Interest

The authors declare that there are no conflicts of interest.

Authors' Contributions

Z.W. and C.C. designed and administered the experiments. C.C. and Z.M. performed the experiments. All authors discussed the data and wrote the manuscript.

Acknowledgments

The authors are grateful to the inorganic functional material group of Shihezi University. The authors also acknowledge Shihezi University for the necessary support provided for the material characterization. This work was supported by the Natural Science Foundation of China (21566031 and 21766029) and the Scientific Research Program of Shihezi University (RCZX201411).

References

[1] R. Shang, X. Guo, S. Mu et al., "Carbon dioxide reforming of methane to synthesis gas over Ni/Si_3N_4 catalysts," *International Journal of Hydrogen Energy*, vol. 36, no. 8, pp. 4900–4907, 2011.

[2] Z. Wang, H. Wang, and Y. Liu, "$La_{1-x}Ca_xFe_{1-x}Co_xO_{3-a}$ stable catalyst for oxidative steam reforming of ethanol to produce hydrogen," *RSC Advances*, vol. 3, no. 25, pp. 10027–10036, 2013.

[3] S. Kawi, Y. Kathiraser, J. Ni, U. Oemar, Z. Li, and E. T. Saw, "Progress in synthesis of highly active and stable nickel-based catalysts for carbon dioxide reforming of methane," *Chemsuschem*, vol. 8, no. 21, pp. 3556–3575, 2015.

[4] A. Pietraszek, B. Koubaissy, A.-C. Roger, and A. Kiennemann, "The influence of the support modification over Ni-based catalysts for dry reforming of methane reaction," *Catalysis Today*, vol. 176, no. 1, pp. 267–271, 2011.

[5] A. Tsoukalou, Q. Imtiaz, S. M. Kim, P. M. Abdala, S. Yoon, and C. R. Müller, "Dry-reforming of methane over bimetallic $Ni–M/La_2O_3$ (M=Co, Fe): the effect of the rate of $La_2O_2CO_3$ formation and phase stability on the catalytic activity and stability," *Journal of Catalysis*, vol. 343, pp. 208–214, 2016.

[6] Z. Shang, S. Li, L. Li, G. Liu, and X. Liang, "Highly active and stable alumina supported nickel nanoparticle catalysts for dry reforming of methane," *Applied Catalysis B: Environmental*, vol. 201, pp. 302–309, 2017.

[7] N. Wang, K. Shen, L. Huang, X. Yu, W. Qian, and W. Chu, "Facile route for synthesizing ordered mesoporous Ni–Ce–Al oxide materials and their catalytic performance for methane dry reforming to hydrogen and syngas," *ACS Catalysis*, vol. 3, no. 7, pp. 1638–1651, 2013.

[8] J. Dou, Z. Bao, and F. Yu, "Mesoporous $Ni(OH)_2/CeNi_xO_y$ composites derived $Ni/CeNi_xO_y$ catalysts for dry reforming of methane," *Chemcatchem*, vol. 10, no. 1, 2018.

[9] M. Wang, T. Zhao, X. Dong, M. Li, and H. Wang, "Effects of Ce substitution at the A-site of $LaNi_{0.5}Fe_{0.5}O_3$ perovskite on the enhanced catalytic activity for dry reforming of methane," *Applied Catalysis B: Environmental*, vol. 224, pp. 214–221, 2018.

[10] Z. Bian, I. Y. Suryawinata, and S. Kawi, "Highly carbon resistant multicore-shell catalyst derived from Ni-Mg phyllosilicate nanotubes@silica for dry reforming of methane," *Applied Catalysis B: Environmental*, vol. 195, pp. 1–8, 2016.

[11] X. Du, D. Zhang, L. Shi, R. Gao, and J. Zhang, "Morphology dependence of catalytic properties of Ni/CeO_2 nanostructures for carbon dioxide reforming of methane," *The Journal of Physical Chemistry C*, vol. 116, no. 18, pp. 10009–10016, 2012.

[12] X. Du, D. Zhang, R. Gao, L. Huang, L. Shi, and J. Zhang, "Design of modular catalysts derived from NiMgAl-LDH@m-SiO_2 with dual confinement effects for dry reforming of methane," *Chemical Communications*, vol. 49, no. 60, pp. 6770–6772, 2013.

[13] J. H. Park, S. Yeo, T. J. Kang, H. R. Shin, I. Heo, and T. S. Chang, "Effect of Zn promoter on catalytic activity and stability of Co/ZrO_2 catalyst for dry reforming of CH_4," *Journal of CO_2 Utilization*, vol. 23, pp. 10–19, 2018.

[14] Z. Liu, D. C. Grinter, P. G. Lustemberg et al., "Dry reforming of methane on a highly-active $Ni-CeO_2$ catalyst: effects of metal-support interactions on C-H bond breaking," *Angewandte Chemie International Edition*, vol. 55, no. 26, pp. 7455–7459, 2016.

[15] Y.-J. Su, K.-L. Pan, and M.-B. Chang, "Modifying perovskite-type oxide catalyst $LaNiO_3$ with Ce for carbon dioxide reforming of methane," *International Journal of Hydrogen Energy*, vol. 39, no. 10, pp. 4917–4925, 2014.

[16] L. Li, P. Lu, Y. Yao, and W. Ji, "Silica-encapsulated bimetallic Co–Ni nanoparticles as novel catalysts for partial oxidation of methane to syngas," *Catalysis Communications*, vol. 26, no. 35, pp. 72–77, 2012.

[17] M. Ocsachoque, F. Pompeo, and G. Gonzalez, "Rh–Ni/CeO_2–Al_2O_3 catalysts for methane dry reforming," *Catalysis Today*, vol. 172, no. 1, pp. 226–231, 2011.

[18] T. Odedairo, J. Chen, and Z. Zhu, "Metal–support interface of a novel Ni–CeO_2 catalyst for dry reforming of methane," *Catalysis Communications*, vol. 31, no. 2, pp. 25–31, 2013.

[19] X. Xie, T. Otremba, P. Littlewood, R. Schomäcker, and A. Thomas, "One-pot synthesis of supported, nanocrystalline nickel manganese oxide for dry reforming of methane," *ACS Catalysis*, vol. 3, no. 2, pp. 224–229, 2013.

[20] Y. Han, B. Wen, and M. Zhu, "Core-shell structured Ni@SiO_2 catalysts exhibiting excellent catalytic performance for syngas methanation reactions," *Catalysts*, vol. 7, no. 12, p. 21, 2017.

[21] A. I. Paksoy, B. S. Caglayan, E. Ozensoy, A. N. Ökte, and A. E. Aksoylu, "The effects of Co/Ce loading ratio and reaction conditions on CDRM performance of $Co-Ce/ZrO_2$ catalysts," *International Journal of Hydrogen Energy*, vol. 43, no. 9, pp. 4321–4334, 2018.

[22] X. Zheng, S. Tan, L. Dong, S. Li, and H. Chen, "Plasma-assisted catalytic dry reforming of methane: highly catalytic

performance of nickel ferrite nanoparticles embedded in silica," *Journal of Power Sources*, vol. 274, pp. 286–294, 2015.

[23] L. Xu, F. Wang, M. Chen et al., "Carbon dioxide reforming of methane over cobalt-nickel bimetal-doped ordered mesoporous alumina catalysts with advanced catalytic performances," *Chemcatchem*, vol. 8, no. 15, pp. 2536–2548, 2016.

[24] S. Wu, Y. Lin, C. Yang et al., "Enhanced activation of peroxymonosulfte by $LaFeO_3$ perovskite supported on Al_2O_3 for degradation of organic pollutants," *Chemosphere*, vol. 237, Article ID 124478, 2019.

[25] Y. A. Daza, D. Maiti, B. J. Hare, V. R. Bhethanabotla, and J. N. Kuhn, "More Cu, more problems: decreased CO_2 conversion ability by Cu-doped $La_{0.75}Sr_{0.25}FeO_3$ perovskite oxides," *Surface Science*, vol. 648, pp. 92–99, 2016.

[26] E.-H. Yang, Y.-S. Noh, S. Ramesh, S. S. Lim, and J. M. Dong, "The effect of promoters in $La_{0.9}M_{0.1}Ni_{0.5}Fe_{0.5}O_3$ (M=Sr, Ca) perovskite catalysts on dry reforming of methane," *Fuel Processing Technology*, vol. 134, pp. 404–413, 2015.

[27] S. Zhuang, Y. Liu, S. Zeng, J. Lv, X. Chen, and J. Zhang, "A modified sol–gel method for low-temperature synthesis of homogeneous nanoporous $La_{1-x}Sr_xMnO_3$ with large specific surface area," *Journal of Sol-Gel Science and Technology*, vol. 77, no. 1, pp. 109–118, 2016.

[28] R. C. R. Neto, H. B. E. Sales, C. V. M. Inocêncio et al., "CO_2 reforming of methane over supported $LaNiO_3$ perovskite-type oxides," *Applied Catalysis B: Environmental*, vol. 221, pp. 349–361, 2018.

[29] J. Hwang, R. R. Rao, L. Giordano, Y. Katayama, Y. Yu, and Y. Shaohorn, "Perovskites in catalysis and electrocatalysis," *Science*, vol. 358, no. 6364, pp. 751–756, 2017.

[30] Z. Wang, C. Wang, S. Chen, and Y. Liu, "Co–Ni bimetal catalyst supported on perovskite-type oxide for steam reforming of ethanol to produce hydrogen," *International Journal of Hydrogen Energy*, vol. 39, no. 11, pp. 5644–5652, 2014.

[31] Y. Chai, Y. Fu, H. Feng et al., "Ni-based perovskite catalyst with a bimodal size distribution of Ni particles for dry reforming of methane," *Chemcatchem*, vol. 10, no. 9, 2018.

[32] S. M. D. Lima and J. M. Assaf, "Ni–Fe catalysts based on perovskite-type oxides for dry reforming of methane to syngas," *Catalysis Letters*, vol. 108, no. 1-2, pp. 63–70, 2006.

[33] X. Li, H. Shi, W. Zhu et al., "Nanocomposite $LaFe_{1-x}Ni_xO_3$/Palygorskite catalyst for photo-assisted reduction of NO_x: effect of Ni doping," *Applied Catalysis B: Environmental*, vol. 231, pp. 92–100, 2018.

[34] G. S. Gallego, F. Mondragón, J. Barrault, J. M. Tatibouët, and C. Batiot-Dupeyrat, "CO_2 reforming of CH_4 over La–Ni based perovskite precursors," *Applied Catalysis A: General*, vol. 311, no. 3, pp. 164–171, 2006.

[35] I. Rivas, J. Alvarez, E. Pietri, M. J. Pérez-Zurita, and M. R. Goldwasser, "Perovskite-type oxides in methane dry reforming: effect of their incorporation into a mesoporous SBA-15 silica-host," *Catalysis Today*, vol. 149, no. 3, pp. 388–393, 2010.

[36] N. Wang, C. Wei, T. Zhang, and X. S. Zhao, "Synthesis, characterization and catalytic performances of Ce-SBA-15 supported nickel catalysts for methane dry reforming to hydrogen and syngas," *International Journal of Hydrogen Energy*, vol. 37, no. 1, pp. 19–30, 2012.

[37] H. Wu, H. Liu, W. Yang, and D. He, "Synergetic effect of Ni and Co in Ni-Co/SBA-15-CD catalysts and their catalytic performance in carbon dioxide reforming of methane to syngas," *Catalysis Science & Technology*, vol. 6, no. 14, pp. 5631–5646, 2016.

[38] N. Wang, K. Shen, X. Yu, W. Qian, and W. Chu, "Preparation and characterization of a plasma treated NiMgSBA-15 catalyst for methane reforming with CO_2 to produce syngas," *Catalysis Science & Technology*, vol. 3, no. 9, pp. 2278–2287, 2013.

[39] S. Afzal, X. Quan, and J. Zhang, "High surface area mesoporous nanocast $LaMO_3$ (M = Mn, Fe) perovskites for efficient catalytic ozonation and an insight into probable catalytic mechanism," *Applied Catalysis B: Environmental*, vol. 206, pp. 692–703, 2017.

[40] A. Zhang, A. Zhu, B. Chen, S. Zhang, C. Au, and C. Shi, "In-situ synthesis of nickel modified molybdenum carbide catalyst for dry reforming of methane," *Catalysis Communications*, vol. 12, no. 9, pp. 803–807, 2011.

[41] H. Messaoudi, S. Thomas, A. Djaidja, S. Slyemi, and A. Barama, "Study of LaxNiOy and $La_xNiO_y/MgAl_2O_4$ catalysts in dry reforming of methane," *Journal of CO_2 Utilization*, vol. 24, pp. 40–49, 2018.

[42] B. Zhao, B. Yan, S. Yao et al., "$LaFe_{0.9}Ni_{0.1}O_3$ perovskite catalyst with enhanced activity and coke-resistance for dry reforming of ethane," *Journal of Catalysis*, vol. 358, pp. 168–178, 2018.

[43] U. Oemar, P. S. Ang, K. Hidajat, and S. Kawi, "Promotional effect of Fe on perovskite $LaNi_xFe_{1-x}O_3$ catalyst for hydrogen production via steam reforming of toluene," *International Journal of Hydrogen Energy*, vol. 38, no. 14, pp. 5525–5534, 2013.

[44] Z. Lin, H. Tong, W. Hong, L. Zhang, and L. Yuan, "Ni-Co alloy catalyst from $LaNi_{1-x}Co_xO_3$ perovskite supported on zirconia for steam reforming of ethanol," *Applied Catalysis B: Environmental*, vol. 187, pp. 19–29, 2016.

[45] S. Y. Foo, C. K. Cheng, T.-H. Nguyen, and A. A. Adesina, "Kinetic study of methane CO_2 reforming on Co–Ni/Al_2O_3 and Ce–Co–Ni/Al_2O_3 catalysts," *Catalysis Today*, vol. 164, no. 1, pp. 221–226, 2011.

[46] Y. Zhao, H. Li, and H. Li, "NiCo@SiO_2 core-shell catalyst with high activity and long lifetime for CO_2 conversion through DRM reaction," *Nano Energy*, vol. 45, pp. 101–108, 2018.

[47] S. Zhang, S. Muratsugu, N. Ishiguro, and M. Tada, "Ceria-Doped Ni/SBA-16 catalysts for dry reforming of methane," *ACS Catalysis*, vol. 3, no. 3, pp. 1855–1864, 2013.

[48] Q. Zhang, T. Wu, P. Zhang et al., "Facile synthesis of hollow hierarchical Ni/g-Al_2O_3 nanocomposites for methane dry reforming catalysis," *RSC Advances*, vol. 4, no. 93, pp. 51184–51193, 2014.